5-11-2021

Reliability of SFRP-Strengthened RC Bridge Columns Subjected to Blast Loads

Ahmad Alsendi
Wayne State University, ahmad.alsendi@wayne.edu

Christopher D. Eamon
Wayne State University, eamon@eng.wayne.edu

Reliability of SFRP-Strengthened RC Bridge Columns Subjected to Blast Loads

Ahmad Alsendi[1] and Christopher D. Eamon[2]

Abstract

The reliability of reinforced concrete bridge columns strengthened with externally bonded, steel-fiber reinforced polymer fabric subjected to blast loads was investigated. Columns were modeled with a nonlinear finite element approach that considers material damage, fracture, and separation. Different concrete strengths, longitudinal reinforcement ratios, and gravity and blast load levels were considered, while uncertainties in material strength and stiffness parameters, as well as load characteristics, were incorporated in the probabilistic analysis. It was found that the use of SFRP can allow significant increases in blast load while maintaining the same level of column reliability.

Author Keywords:

reliability, FRP, SFRP, concrete, columns, bridges, finite element analysis, blast

----

1. Ph.D. candidate, Department of Civil & Environmental Engineering, Wayne State University, Detroit, MI, USA (corresponding author); ahmad.alsendi@wayne.edu
2. Associate Professor, Department of Civil & Environmental Engineering, Wayne State University, Detroit, MI, USA; eamon@eng.wayne.edu

Introduction

The vast majority of highway bridges in the United States are designed according to the minimum standards given in the American Association of State Highway and Transportation Officials *LRFD Bridge Design Specifications* (AASHTO LRFD 2017). It is mandated that State Departments of Transportation (DOTs) follow these specifications for the design of new bridges that are fully or partially funded with Federal aid. AASHTO LRFD specifies various loads to which bridge structures must be designed, including dead load, vehicular and pedestrian live load, as well as wind, earthquake, and less frequent loads resulting from other special scenarios. These individual loads are grouped within multiple load combination limit states, which specify which loads must be considered simultaneously and with what corresponding load factors. Within the Extreme Event II limit state, the most recent edition of AASHTO LRFD (AASHTO LRFD 2017) also specifies blast loading. Other extreme loads within this limit state are ice loads and vehicle and vessel collisions, which are to be considered independently. Although AASHTO specifies a limit state combination with blast load, no blast-related design provisions are given, nor are criteria for determining whether a structure should be designed for blast, a decision which is left to the designer. Rather, the specifications only note that, if a bridge is to be designed for blast load, consideration should be given to charge characteristics such as size and shape and modes of delivery.

Although any bridge component is potentially susceptible to damage from blast load, such as the deck and girders as well as the supporting piers, abutments, and foundation, of primary concern and focus of this study are the central piers (columns) common to multi-span structures that bridge divided highways. These central piers are not only readily accessible, but if damaged severely enough to cause a failure, the ends of both spans that they support will collapse. Since there is no requirement in AASHTO to design bridges to resist blast loads, nearly all existing bridge columns have been designed without regard to blast. Neglecting blast load is perhaps reasonable for the large majority of structures, which may be subjected to an extremely small probability of experiencing this load effect within their design lifetime. However, for bridges that are deemed susceptible to credible blast threats, engineers must look beyond AASHTO LRFD for an appropriate design approach.

This lack of codified guidance has been identified by various researchers, who have subsequently addressed different aspects of this problem, where bridge components such as decks (Foglar et al. 2017; Foglar and Kovar 2013; Lawver et al. 2003), girders (Cofer et al 2010; Anwarul Islam and Yazdani 2008), a bridge structural system (Winget et al. 2005), and bridge columns (Williamson et al. 2011a, b; Williams and Williamson 2011) were considered. For columns, the consensus was that blast resistance was most affected by construction geometry and reinforcement parameters such as spacing and splice locations. In general, several different column failure modes were observed, such as base concrete crushing and/or shearing; reinforcement rupture; spalling; and plastic hinging (Winget et al. 2005; Yi et al. 2014a, b). These results have been used to suggest design approaches for blast-resistant bridge columns.

Rather than the design of new columns, this study is concerned with the large inventory of existing bridge columns that were not designed for blast mitigation. If such a structure is determined to require blast protection due to an increased threat level, one possibility would be to replace the existing piers with a new, blast resistant design. However, this option is not only highly disruptive to traffic but costly. A much less expensive and minimally disruptive approach may be to strengthen rather than replace the existing columns. This possibility was investigated by several researchers, including Malvar et al. (2007), who found that column shear capacity was increased under blast load when retrofitted with steel jacketing or wrapped with composite fabric. Fujikura and Bruneau (2011) similarly investigated steel-jacketed columns subjected to blasts and determined that such columns typically failed in base shear, while Heffernan et al. (2011) conducted blast tests on columns wrapped with composite fabric containing either steel or carbon fibers. This latter study found that carbon fiber as well as steel reinforced polymer (SFRP) fabric enhanced blast capacity by reducing concrete crushing near regions of plastic hinging. Later, Eamon and Alsendi (2020) modeled a series of SFRP-strengthened columns subjected to blasts, and similarly found that resistance could be increased. Recognizing that significant uncertainties exist in load and resistance parameters, several studies examined reinforced concrete (RC) column reliability under various blast load scenarios (Hao et al. 2010; Shi and Stewart 2015; Thomas and Sorensen 2018). In a topic related to this study, Hao et al. (2016) estimated the reliability of RC columns externally reinforced with high strength FRP (2280 MPa) and found that such material could effectively increase reliability.

Of the various strengthening options available, the focus of this study is the use of SFRP, which is significantly less expensive than CFRP as well as ductile. As with any composite fabric, an added benefit over a steel jacking approach is that externally-bonded SFRP does not substantially increase column width. As discussed above, only a few studies have considered the effect of SFRP on column blast resistance, and the reliability of such columns remains unquantified. Given that the AASHTO LRFD Specifications were probabilistically calibrated to provide a minimum reliability index of 3.5 for elements designed by these standards, a reliability-based approach for evaluating SFRP-strengthened columns to account for the inherent uncertainties in loads and resistance is appropriate.

Therefore, the objective of this study is to estimate the reliability of a typical RC bridge column retrofitted with externally-bonded SFRP when subjected to blast load, and to compare the reliability results to unprotected columns. Results can be used to assess the effectiveness of SFRP wrapping considering uncertainties, as well as to quantify the column design characteristics needed to achieve a desired level of reliability under a given blast load, such as that specified by AASHTO LRFD. In this process, a reliability model is constructed with key parameters taken as random variables, then column resistance is assessed with a numerical (finite element) approach suggested by Eamon and Alsendi (2020) that was validated to experimental data. The influence of several design parameters, such as concrete strength, amount of reinforcement, axial load, and use of SFRP, on column reliability is then determined.

Columns Considered

The bridge and column design considered are shown in Figures 1 and 2. The exact configuration of the bridged is not critical to this study, and it is used only to obtain reasonable estimations of dead load on the column. Although a wide variety of column designs exist, characteristics of the considered column are based on typical bridge designs used by the Michigan DOT (Eamon et al. 2018). These columns are very similar to those used in other states as well, where common rectangular bridge pier columns are square with edge dimension ranging from 760 to 914 mm and heights from about 3 to 5 m. Typically, multiple columns support a pier cap, which is used as a support beam upon which the ends of the bridge girders rest. In this study, the upper range of column size, 914 mm square and 5 m unsupported length, was considered for analysis, to represent the larger range of common bridge designs which are perhaps more prone to blast attack.

Concrete compressive strengths ($f'c$) of 28 MPa, 42 MPa, and 55 MPa were considered, along with three longitudinal reinforcement ratios (ρ) of 0.015, 0.029, and 0.042. As shown in Figure 2, longitudinal reinforcement consists of 24 bars (7 bars per face), where bar area was varied to produce the reinforcement ratios given above. Keeping the number of bars constant, this would amount to using #8 (25 mm), #11 (35 mm), and #14 (43 mm) bar sizes. Note that the larger bar sizes are not commonly used in construction for typical bridge columns, but were considered to examine the effect of a reasonable range of reinforcing ratio on column reliability. Typical #4 (13 mm) stirrup ties were spaced at 300 mm, a spacing commonly used in the design of bridge pier columns. Reinforcing bars are taken to have yield stress of 414 MPa, with concrete cover of 50 mm.

In cases where SFRP wrap is used, properties are taken from commercially available products (Hardwire 2014). The considered fabric is composed of a 1.2 mm thick polymer sheet which contains unidirectional, high-strength steel strands with yield strength of 985 MPa. In its strong direction, the complete composite sheet has an effective elastic modulus of 66.1 GPa, while in the weak direction, sheet strength and stiffness are structurally insignificant. As with most externally-bonded FRP products, the SFRP sheets are adhered to the column with epoxy resin after appropriate preparation of the concrete surface. Typically, FRP sheets are applied with the strong direction oriented horizontally, with the desire to increase the axial load carrying capacity of an existing column by providing additional confinement. As no specific guidance is codified as to the use of FRP sheets for strengthening columns for blast load, the above application process is assumed to have been followed for the columns considered in this study. Although FRP wrapping is sometimes used for column repair, this is not the purpose investigated in this study. Rather, the concern is to protect an existing, undamaged column from blast load.

Load Models

Bridge dead load effects include those from prefabricated (D_p) and site-cast (D_s) components, as well as from the deck wearing surface (D_w). Nominal dead loads on the column were determined assuming that the central pier supports the ends of two bridge spans, where each span is 18.3 m long and 13 m wide as shown in Figure 1, representing a typical two-lane bridge deck. The reinforced concrete deck is taken to be 228 mm thick and is supported by seven steel girders (W36x170) spaced at 1.9 m. The central pier is composed of four columns that support a 13 m long, 1 m high, and 0.9 m wide pier cap on which the girder bearings rest. This bridge configuration is typical of structures built by the Michigan DOT as well as other state DOTs (Eamon et al. 2018).

Bias factor λ (ratio of mean to nominal value) and coefficient of variation (*V*) for dead load random variables are given in Table 1. To maintain consistency with the established reliability level in AASHTO LRFD, dead load random variable statistical parameters are based on those used in the AASHTO LRFD calibration (Nowak 1999), and are taken a normally distributed.

Because axial load on the column was found to affect reliability when exposed to blast, several different axial load levels were considered for comparison, including dead load alone as well as dead load in conjunction with vehicular live load, as discussed in more detail in the results section. For the latter case, vehicular live load statistics are also taken from those developed for the AASHTO LRFD calibration, and are given in Table 1, where a range of statistical parameters were considered that represent maximum traffic loads corresponding to daily maximums to maximums expected throughout the design lifetime (i.e. 75 years). In this case, no dynamic load effect is applied, as it is assumed that the likelihood of a maximum vehicle load passing over the column while at speed, at the same instant a severe blast load occurs, is practically zero. Thus, the vehicular load is assumed to represent static or very slow-moving traffic (such as caused by traffic congestion) on the bridge during the blast event. The sum of dead and live loads was considered to be normal in the AASHTO LRFD calibration (Nowak 1999). Here, the same approach is used for consistency with previously reported reliability levels.

Blast pressure is represented with the CONWEP model (Hyde 1988), which is based on a modified form of the Friedlander Equation fit to experimental data of various blast pressures found from a variety of charge weights and standoff distances (Kingery and Bulmash 1984). An idealized blast pressure curve resulting from this model is shown in Figure 3. The resulting blast pressure at a particular point away from the source is commonly represented with the scaled distance parameter Z, which is a function of the explosive weight and distance: $Z = R / W^{1/3}$, where R is the distance from the blast initiation point to the column face (m), and W is the explosive weight, in terms of equivalent mass of TNT (kg). Although statistical data describing typical charge standoff distances from blast threats to bridge columns are unavailable, the author inspected approximately 100 bridges damaged from blasts in Iraq from 2014-2016, where a large variation in apparent standoff distance was observed. Based on these inspections, the mean charge placement is taken as 1 m away from the column, with a 50 mm height above the ground surface. Two random variables are used to describe the uncertainty in scaled distance: the effective charge weight (Q_w) and the resulting blast pressure equivalency (Q_e), where Q_w has a Gaussian distribution and Q_e a triangular distribution. Statistics for these parameters are taken from Shi and Stewart (2015), and are provided in Table 1. Since the shock wave generated from the blast load may strike the ground, the blast is modeled as a hemispherical surface burst that includes the reflected shock wave.

Resistance Model

The FEA approach used to evaluate column capacity is taken from Alsendi and Eamon (2020), which was used to model columns very similar to those considered here, and was reported to well-match experimental data. In this approach, concrete is modeled with the Johnson-Holmquist-Cook approach, which was specifically formulated for the large strains, high strain rates, and high pressures associated with blast loads. Here, material strength is a function of pressure, strain rate, and cumulative damage caused by pressure and plastic strains. The sixteen specific material constants needed to define the model are taken from Alsendi and Eamon (2020), which are based on values experimentally determined from tests conducted by Holmquist et al. 1993 and Williamson et al. 2010 for concrete strengths similar to those used in this study.

The constitutive relationship of reinforcing steel is represented by a kinematic, elastic-plastic model, where nominal yield stress is taken as 414 MPa, Young's modulus 200 GPa, and post-yield modulus 20 GPa. The Copwer and Symonds approach (Livermore Software Technology Corporation 2018) is used for strain-rate strengthening, where yield stress is factored by the relationship: $1 + \left(\frac{\dot{\varepsilon}}{C}\right)^{1/p}$. In this expression, $\dot{\varepsilon}$ is the strain rate, and *c* and *p* are material-specific parameters, taken as 40.4 s^{-1} and 5.0, respectively (Bai and Jin 2016).

An anisotropic model is used to characterize the SFRP sheet, with Young's modulus and yield stress nominally taken as 66.1 GPa and 985 MPa in the strong direction, with a Poisson ratio of 0.30, and approximately 1/100th of these values in the weak direction, where strength and stiffness are insignificant (Hardwire 2014). Based on typical resin properties, the SFRP bond is modeled with a shear strength of 32 MPa and a normal (tensile) strength of 29.4 MPa (Sikadur 2017).

Using these material models, approximately 171,000 hexahedral elements were used to model the column concrete, with element length ranging from 14 to 25 mm. Reinforcing bars were modeled with beam elements, and, prior to concrete failure/crushing, are assumed to be fully bonded to the concrete. To model debris resulting from fracturing as well as to avoid greatly distorted elements in the analysis, once the principal strain of a concrete element reaches 0.003 or greater, it is assumed to be completely crushed/fractured and deleted from the mesh. In general, elements so greatly strained have insignificant remaining strength and stiffness per the material softening model used above. If an element surface is exposed due to the elimination of adjoining elements, a new contact surface is generated to prevent the penetration of potentially colliding elements. Similar surfaces are used on reinforcing bar elements.

The SFRP was modeled with shell elements. For the columns considered, the SFRP was only applied to the lower half of the column (wrapped around all sides), where blast load was greatest. It was found that wrapping the entire height of the column with SFRP increased computational time but made little difference to column blast resistance when compared to results from the half-height wrapping. This is not surprising, since failure generally occurs at the column base, as discussed in more detail below.

Similar to the reinforcing bar elements, contact surfaces are used to link the SFRP elements to the concrete elements, allowing potential element collision if elements become detached. The SFRP contact surface, which represents the resin bond between the concrete and composite wrapping, is assumed to link the SFRP to the concrete without slip, prior to failure. However, once the bond failure criteria is reached, the link between the SFRP shells and concrete solid elements is released, allowing the possibility of sliding or contact. The bond failure criteria is given as the vector sum of the ratios of the calculated normal (tensile) and shear stresses to the normal and tensile failure stresses, where summations greater than unity indicate bond failure. Further, if a SFRP element reaches a longitudinal strain limit (in the strong direction) of 0.021, fiber rupture is expected (Hardwire 2014). In this case, the SFRP element is deleted from the model.

To represent a typical bridge column, which is poured integral with a reinforced concrete foundation, its base was taken as fixed (all nodal degrees of freedom constrained at the ground level). The top of the column was attached to a simple frame (beam element) model of the pier cap and adjoining columns to provide an equivalent lateral constraint stiffness, using stiffness properties based on the member geometries given above.

These models were explicitly solved with a large strain, large displacement Lagrangian FEA approach that allows element disintegration, separation, and contact, as implemented in LS-DYNA (Livermore Software Technology Corporation 2018), using the approach described above.

As reported by Alsendi and Eamon (2020), this FEA modeling approach was found to well-represent experimental results of similar columns exposed to blast loads. An example comparison of the model to a typical test result is given in Figure 4, where the overall deformed shape, magnitude of displacement, concentration of cracks, and locations of spalled concrete appear to be reasonably represented. Particularly important is the ability of the model to represent the behavior of the column base, where failure occurs. As shown in Figure 4, the model result reasonably matches the deformation angle and displacement of the column base, as perhaps seen most clearly from the exposed reinforcing bars that are on the right side of the column. The test column was similar in form but slightly smaller than those considered in this study, with height of 3.43 m and otherwise identical to the section shown in Figure 2, except each side length is 760 mm. This column had 28.6 MPa concrete strength and seven, 19 mm (#6) longitudinal bars per face and 13 mm (#4) stirrup ties with spacing of 150 mm and 25 mm cover. The longitudinal bars and ties had yield strength of 450 and 345 MPa, respectively. The column had a fixed base and pinned top with no axial load.

To select appropriate resistance random variables, a preliminary investigation was conducted and determined that reliability results were relatively insensitive to variables representing geometric uncertainties (column width, rebar area, FRP sheet thickness), based on random variable statistical parameters reported in the literature (Nowak and Szerszen 2003; Behnam and Eamon 2013; Ellingwood et al. 1980; Atadero and Karbhari 2008). The remaining, most influential resistance random variables are material strength and stiffness parameters, and include concrete compressive strength (f'_c); yield stress of the longitudinal bars (F_{yl}), stirrup ties (F_{yt}), and SFRP (F_{yS}); Young's modulus of the longitudinal bars (E_l), stirrup ties (E_t), and SFRP (E_S); and tangent modulus of the longitudinal bars (E_{Tl}), stirrup ties (E_{Tt}), and SFRP (E_{Ts}). In the model, all strength (and stiffness) random variables were initially taken as independent among separate reinforcing bars. However, it was found that the level of correlation between stirrup tie properties did not significantly influence results, and these were thus taken as fully correlated to simplify the reliability model. This resulted in 24 random variables each for yield stress, elastic modulus, and tangent modulus to describe uncertainties in the 24 longitudinal bars, and one random variable for each of these three parameters to describe all stirrup ties, and two random variables to decribe the SFRP fabric. This resulted in 79 resistance random variables (3 RVs F_{yl}, E_l, and E_{Tl} for each of the 24 bars, and 1 additional RV for f'_c, F_{yt}, F_{yS}, E_t, E_S, E_{Tt}, and E_{Ts}) as summarized in Table 1. Statistical parameters are taken from Nowak and Szerszen (2003), Wisniewski et al. (2012), and Val and Chernin (2009). All are reported as normally distributed.

Reliability Analysis

The limit state function is written in terms of the axial load capacity of the column, where failure is defined as the event where the column can no longer support the axial load imposed and begins to collapse (while subjected to the blast load described above). The resulting limit state function can be expressed as: $g = f(\boldsymbol{X_i})$, where $g < 0$ corresponds to column collapse. Random variables $\boldsymbol{X_i}$ are identified in Table 1, and g is not written in closed form but must be evaluated implicitly with the finite element procedure described above. Various methods are available for assessing reliability, including reliability-index based approaches (Rackwitz and Fiessler 1978; Nowak and Nowak 2008), simulation methods (Au and Beck 2001; Rocha et al. 2011), as well as other techniques (Gomes and Awruch 2004; Acar et al. 2008). For this study, the high computational demand of the model coupled with the relatively high reliability indices in some of the cases explored required an accurate method with reasonable computational cost. It was found that the most probable point of failure (MPP) could not be located for this problem, prohibiting the use of the highly efficient reliability-index based methods, whereas direct Monte Carlo simulation (MCS) is too costly for the accuracy desired. Thus, failure probability was computed with the Failure Sampling method, an alternative approach specifically developed for efficient evaluation of complex, moderate to high reliability problems. Described in detail elsewhere (Eamon et al. 2020), a brief description of the process is as follows:

1. The initial limit state function $g(\boldsymbol{X_i})$ is rewritten as g^*. g^* is expressed in terms of a control random variable, taken as Q_w, and the function of remaining RVs, $R(\boldsymbol{X_j})$. Setting g^* to zero to represent the failure boundary, the problem is alternatively expressed as:

$$g^* = R(\boldsymbol{X_j}) - Q_w = 0 \qquad (1)$$

In Eq. 1, g^* is mathematically equivalent to original limit state function g. Note that function $R(\boldsymbol{X}_j)$ is not explicitly formed as it is evaluated from the FEA model.

2. For a particular simulation, values for RVs within $R(\boldsymbol{X}_j)$ are determined by MCS, then the required value for Q_w necessary to satisfy Eq. 1 is determined. Because $R(\boldsymbol{X}_j)$ is implicit, a nonlinear solver is required to determine this value. That is, Eq. 1 is solved by incrementing Q_w with the FEA procedure until the simulated column can just no longer support its axial load.

3. The simulation process (step 2) is repeated until the desired sample size is generated. For each simulation, the FEA model is updated with the simulated values of the RVs given in Table 1. A program was written to automate the procedure of generating the random values via MCS, inserting these values into the FEA input file, running the FEA code, extracting results, incrementing the control variable for nonlinear solution of Q_w, and repeating the process for subsequent simulations. In this study, 1000 simulations were used. This choice is further discussed below.

4. Since $R(\boldsymbol{X}_j) = Q_w$ on the failure boundary, the values determined for Q_w also must equal corresponding values for $R(\boldsymbol{X}_j)$. Thus, the (1000-point) data sample reduces the complex, high-dimensional function $R(\boldsymbol{X}_j)$ into that describing a single representative random variate R. Due to the sparsity of data in the critical tail region of $R(\boldsymbol{X}_j)$ when solving the column scenarios that have high reliability, the data sample is further represented with an analytical curve that can be used to extend the tail region indefinitely. Since the accuracy of the reliability solution depends on how well the actual distribution of R is modeled, the curve representing the CDF of R is developed from an ensemble of three highly-flexible, three and four-parameter distributions: the generalized lambda distribution (GLD), Johnson's distribution (JSD), and the generalized extreme value distribution (GEV). Although each curve is relatively flexible by itself, the resulting hybrid CDF

takes advantage of the combined ability of all three curves to best match *R*. To determine how the curves are optimally combined, the individual CDFs are assigned weight factors depending upon their anticipated accuracy. Using a weighted sum formulation, a unique, problem-specific ensemble of CDFs is formulated as: $F_{RE} = \sum_{i=1}^{3} w_i F_{RTi}$, where F_{RE} is the final ensemble CDF of the three stand-alone CDFs F_{RTi}, and w_i is the weight factor of *ith* stand-alone CDF. The weight factors are determined by a sequential quadratic programming optimization process where the difference between the CDF formed directly from the 1000 sampled datum points, the "true" CDF, given as: $F_R(s) = s / (1000 + 1)$, and the analytical representation, F_{RE}, is minimized, where $F_R(s)$ is the CDF value for datum *s*. The error between the true CDF and F_{RE} is measured using generalized mean square error. The final optimized ensemble CDF of resistance is thus used to represent *R*. An example curve used to represent *R* for a typical column exposed to blast is given in Figure 5. As shown, the optimized curve is dominated by the GEV in this case (with corresponding curve weights $w_{GEV} = 0.91$; $w_{GLD} = 0.08$; $w_{JSD} = 0.01$).

5. Since *Q* is an RV with known parameters, Eq. 1. can now be explicitly expressed as: $g^* = R - Q$. This simple, analytical, two RV limit state function can then be readily solved with any reliability method as desired. In this study, direct MCS was used (from approximately $1\text{x}10^6$-$1\text{x}10^8$ simulations, as appropriate for the reliability level evaluated).

It is important to note that this process is not a simple curve fit to the limit state function *g*, which would require a much larger data sample to produce an accurate representative single variate *G*. The effectiveness of the method relies on separating *R* and *Q* to identify points on the failure boundary. As demonstrated in Patki and Eamon (2016), this allows defining a region within *g* much closer to the failure region, which requires much fewer points to define accurately, than *g* as a whole. Thus, sufficient data are only needed to define the shape of *R* rather than to attempt to capture failures of *g*. This concept is shown in Figure 6. The sample size needed to do this effectively for a variety of problems has been discussed by Eamon and Charumas (2011). As expected, increasing the number of simulations typically leads to greater accuracy. However, 1000 was recommended for most problems, even if using a single curve rather than an ensemble, as a reasonable balance between computational effort and accuracy. To verify the appropriateness of a 1000-point data sample for this specific problem in this study, several columns exposed to different blast loads to produce reliability indices between approximately -0.5 to 3.8 were modeled. To allow for feasible validation, the mesh of these columns was coarsened and the analysis stopped once a displacement limit was met that was predictive of column failure rather than complete collapse. These simplifications were found to reasonably approximate the behavior of the original models, and could be feasibly solved with MCS using up to $1x10^5$ simulations. The validation analysis found that the FS reliability result was within 3% of the direct MCS solution in each case (case 1: β_{MCS}= -0.52; β_{FS} = -0.52; case 2: β_{MCS}= 2.65; β_{FS} = 2.65; case 3: β_{MCS}= 3.89; β_{FS} = 3.80). As this result confirmed the earlier sample size recommendation and was deemed sufficiently accurate for this study, no further changes in the number of simulations were implemented.

Results

To assess column reliability across a variety of small to moderate blast threats, results are presented for a range of scaled distances from approximately 0.1 to 0.3 $m/kg^{1/3}$. A representative column response to blast is given in Figure 7. Typically, when the peak overpressure on the column face is reached, the base of the column is pushed laterally from the blast, producing extensive cracking at the base. Although this does not represent a traditional concrete shear failure due to the very steep (nearly parallel to the lateral blast load) primary crack angle at the very base of the column, this critical crack formation is predominately caused by a shearing distortion, accompanied by high deviatoric stress. This behavior, ultimately the result of excessive concrete strain from shearing and tension, can be clearly seen in the experimental results (see Fig. 4), as well as from the distortion of the reinforcing bars at the base of the FEA model. This displacement causes the column to slightly rotate as the base becomes eccentric to the top, crushing some concrete elements into the load plate used to represent the lower surface of the pier cap. Similar behavior was also reported for concrete masonry walls exposed to blasts (Eamon et al. 2004). The lateral displacement of the base similarly causes yielding of the reinforcing bars. Once the base loses stiffness due to extensive material softening from cracking and bar distortion, the column can no longer offer sufficient support for the axial load imposed and it ultimately collapses.

The cause of failure of a SFRP-strengthened column exposed to blast is similar to the unwrapped case: base failure. The SFRP on the column face (as well as SFRP on a narrow vertical region on the sides of the column closest to the blast-exposed face) is first severely damaged and experiences bond loss and destruction, while SFRP on the remaining column surface areas does not experience significant damage. The column base then soon fails thereafter in the same manner as with the non-wrapped column. SFRP increases blast resistance capacity by providing additional external reinforcement and some enhancement of confinement. It was found that the primary benefit from wrapping, however, with respect to blast resistance, is its reinforcing ability rather than confinement. This was determined by removing the continuity of SFRP by placing four independent, disconnected sheets on the column faces. This resulted in only a minor loss of blast resistance as compared to the continuous sheet (within a few percent), suggesting that confinement provides a measurable, but minor role in resistance. It was also found that the SFRP does not act as reinforcement in the traditional sense, where a fundamental distinction exists between flexure and shear. Rather, changing the strong orientation of the SFRP from the horizontal (acting as shear reinforcement) to vertical (acting as flexural reinforcement) made little difference, where the vertical orientation could resist only slightly less (again within a few percent) blast load effect than the horizontal orientation, suggesting that it serves modestly more effectively as shear reinforcement. This is perhaps expected, given the shear distortion that was observed to cause column failure. Other resistance mechanisms result from the additional mass and ductility of the SFRP sheets that absorb blast energy with their destruction; as well as the ability of the wrapping to simply hold the concrete shell together (when not destroyed) and enable the column to resist spalling, such that it can continue to carry a portion of the axial force as well as continue to protect the concrete core.

Although useful for providing an understanding of column behavior, a drawback of the model discussed above is the large computational effort involved. However, it was found that nearly identical (within a few percent) blast load capacity results could be obtained with a less detailed mesh and by varying mesh density, with concrete element edge sizes of 9.5 cm for elements close to the charge where most cracks appear, and edge sizes of 9.5 cm square and 38 cm high for elements away from the charge. This resulted in only 1090 concrete elements (not including SFRP shells), with a corresponding large decrease in solution time. This less detailed model was used to perform the reliability analysis results detailed below. Although useful for ultimate capacity analysis, this more coarse model loses effectiveness for predicting crack patterns. However, this detailed information is not of further interest to this study.

As the axial load on the column was found to affect reliability under blast, to present a range of possible reliability results, three axial load cases were considered. These are dead load (DL); nominal load (NL); and maximum load (ML). The DL case includes only the self-weight of the structure described above (deck, girders, barriers, diaphragms, and pier cap), and represents the most likely scenario when the column is subjected to blast load. Because traffic live load is highly variable and a function of time and location, appropriate sustained, or arbitrary-point-in-time values for traffic load to be used in conjunction with a transient blast load have not been established. Thus, a variety of live load levels were investigated in this study. Based on the traffic load model used in the AASHTO LRFD calibration (Hardwire 2014), as well as actual traffic data recorded in the State of Michigan (Eamon et al. 2016), typical daily or even yearly maximum loads were found to have little effect on reliabilty under blast, as results are insensitve to changes in axial load above dead load at these relatively low live load levels. To explore this issue further, an extremely heavy mean maximum vehicle load on the bridge was considered, taken as 2450 kN. A traffic load of of this magnitude may represent a yearly maximum special permit vehicle. For example, weigh-in-motion data collected for two years over dozens of major highway in Michigan reported a maximum vehicle weight of 2420 kN (Eamon et al. 2014), from over 66 million vehicle records. Note that a maximum legally loaded common 5-axle tractor-semi trailer truck in most states of the US is about 356 kN; assuming 4 such vehicles on the bridge together, one on each span and in both lanes, results in 1424 kN. This was also found to have minimal impact on reliability. As these loads were found to have little influence on reliabiltiy under blast load, theoretically higher levels of load were considered in order to better understand how reliabilty changes with axial load level. These higher load levels are represented with the NL and ML cases. The former is set equal to the total unfactored load that the column can support, per AASHTO LRFD design criteria. This load would practically apply only to a much larger structure than that shown in Fig 1. The ML case corresponds to applying a load equal to the nominal capacity of the column. Although the latter case represents an unrealistic design scenario, it was studied to establish a bound of possible column performance when subjected to blast.

Reliability results are given in Figures 8-16. Failure probability *(p_f)* results are converted to generalized reliability index β (i.e. $\beta = -\Phi^{-1}(p_f)$) for ease of comparison to established levels of code reliability. For each case, columns were subjected to a range of blast loads such that the resulting reliability indices ranged from about 5 to -1, where positive values indicate $p_f < 0.5$ and negative values represent $p_f > 0.5$. Baseline results can be thought to be represented at the $\beta = 0$ line, where $p_f = 0.50$. That is, this represents the blast load applied that just causes the column to fail, regardless of the accompanying uncertainties; i.e. these load values essentially represent deterministic column capacity results when evaluated using the mean values of the random variables. Note that in any situation where mean load effect exceeds mean resistance, reliability index will fall below zero. In this study, this occurs for cases where the scaled distance Z becomes small and the corresponding blast load effect becomes high, resulting in probable column failure.

Figures 8-10 present results for columns with reinforcement ratios ρ=0.015 for different axial load levels. Considering Figure 8, for columns subjected to axial dead load (DL), as expected, reliability index increases as scaled distance increases (and thus as effective blast load decreases), and the reliability of the bare columns to those wrapped with SFRP tends to converge as blast load is increased. This latter observation is not surprising, since as blast load increases, reliability becomes more dominated by load effect rather than SFRP resistance characteristics.

As noted above, and as expected, increasing concrete strength significantly increases reliability for low to moderate blast loads. Even at $Z = 0.24$ m/kg$^{1/3}$, increasing concrete strength from 28 to 55 MPa results in a corresponding increase in reliability index from about 1 to about 3. As compared to increasing concrete strength, the benefit of SFRP is measurable but less significant. For example, applying SFRP on the 28 MPa column at a scaled distance of 0.24 m/kg$^{1/3}$ increases reliability index from 1 to approximately 2, which is about the same effect as increasing concrete strength from 28 to 42 MPa. Similar to changes in concrete strength, the largest benefits from SFRP occur at low and moderate blast loads.

Comparing results in Figures 8-10, a significant benefit in blast reliability is realized by increasing the mean axial load on the short columns studied here where buckling is not a concern, where enhancements in reliability due to increases in concrete strength or the use of SFRP become more pronounced. For example, considering Z = 0.22 m/kg$^{1/3}$, increasing the axial load from the DL (Figure 8) to NL (Figure 9) cases resulted in increases in reliability index from 0.0 to 0.5 (28 MPa column) and 1.1 to 3.0 (55 MPa column) without SFRP, and from 0.5 to 1.0 (28 MPa column) and 2.0 to 4.0 (55 MPa column) with SFRP. This remains an increasingly beneficial effect as axial load increases to a load approximately equal to the nominal axial capacity of the column. However, this benefit does have limits; it was found that increasing axial load slightly beyond nominal capacity will cause a failure even at very low blast loads, as the column has little reserve capacity remaining to sustain damage of any kind. Here note that the mean axial load capacity, as used in the analysis, is about 15% greater than nominal capacity due to the material strength bias factors shown in Table 1. Although the peak effective load level depends on the specific column properties, applying an axial load large enough to be approximately within the region between nominal and mean capacity becomes detrimental to blast resistance (and of course, applying an axial load beyond mean capacity will cause an immediate failure due to overload). At lower load levels, however, the axial load practically serves as prestressing, lowering tensile stresses and inhibiting the crack development and growth that ultimately causes base failure.

Note that the ML results are provided as theoretical interest only, since such a high axial load level does not represent a realistic scenario. To study the effect of blast damage on remaining column axial capacity in more detail, a column at a more reasonably expected maximum NL load level was considered. Here, a typical column (f'_c = 42 MPa, ρ = 0.029) subjected to the NL load level was exposed to a scaled blast distance that was close too, but below that (approximately Z = 0.20) which would cause failure. Once the blast event was complete and the column reached static equilibrium, the axial load was slowly increased until column collapse occurred.

For an unwrapped column, it was found that the blast-damaged column could maintain approximately 90% of its undamaged maximum axial load. When exposed to an effective blast load of 90% of the original effect (i.e. Z = 0.22), the column could maintain 94% of the undamaged maximum axial load. And when exposed to 50% of the original blast load (Z = 0.40), the column could sustain nearly 98% of its undamaged maximum load. Therefore, the column axial capacity is largely unaffected unless the blast load reaches a relatively high level, close to that which would cause immediate collapse. It thus appears that there is a significantly nonlinear relationship between blast load and column axial capacity.

Wrapping the same column allowed an increase in resistance to blast load effect by approximately 10% (Z = 0.18) as compared to the unwrapped case, though the post-blast column could carry a slightly lower proportion of its maximum axial load (87%, vs 90% for the unwrapped column exposed to a lower blast level). Subjecting the wrapped column to 90% of its initial blast load (Z = 0.20) allowed the post-blast column to resist just slightly more axial load than the unwrapped column exposed to the same blast level (92% vs 90%); and subjecting the wrapped case to 50% of its initial blast load (Z = 0.36) enabled the column to resist 96% of its maximum axial load post-blast (as compared to the unwrapped column, exposed to 50% of its initial blast load at a lower Z of 0.40, which could sustain 98% of its initial maximum load). As shown above, exposing a wrapped column to same load level as an unwrapped case is accompanied by an increase in post-blast capacity, as expected. Within the range of loads considered, the benefit that wrapping provides to post-blast capacity appears to increase at lower blast load levels.

Figures 11-13 and 14-16 are similar to 8-10, except results for columns with higher reinforcement ratios (0.029 and 0.042) are presented. Similar trends are shown, but column reliabilities are generally higher, as expected. For example, again considering a 28 MPa column at $Z = 0.24$ m/kg$^{1/3}$ under the DL load case, reliability indices vary from approximately 1.3 for ρ=0.015, 1.8 for ρ=0.029, and 2.2 for ρ=0.042. In summary, for the columns studied, reliability is most sensitive to changes in concrete strength, SFRP, then longitudinal reinforcement ratio.

As this study concerns reliability due to blast, the results shown consider failures initiated by blast load only, not from extreme gravity loads. That is, any column failure that occurred due to sampling an extreme vehicle overload before the blast load could be applied was removed from the results. For comparison, the effects of extreme gravity loads on column reliability, when not exposed to blast, are given in Table 2. As shown, reliability increases as reinforcement ratio increases and concrete strength decreases. This occurs at the NL and ML load levels because the axial load applied is a function of column capacity (as column capacity increases, axial load is correspondingly increased, per the definition of these load cases given earlier), and the variability of column strength decreases as steel, with its relatively low coefficient of variation, carries proportionally more load than concrete. Perhaps unexpected, this also occurs at the DL load level, where axial load is held constant regardless of column strength. Again, this trend occurs for a similar reason, where the increase in mean column strength is outweighed by the corresponding increase in variability of strength, causing a net increase in failure probability. For example, for the column with $\rho = 0.042$, as concrete strength is increased from 28 to 55 MPa, mean column capacity increased by 57%, but the standard deviation of column strength approximately doubled.

To provide context to the values shown in Table 2, a column designed according the AASHTO LRFD specifications, without overdesign, would correspond to the NL load case. The reliability index is for a reinforced concrete beam designed per AASHTO LRFD is approximately 4 (Nowak 1999). This reported beam reliability index is based on a tension-controlled flexural failure, as opposed to the compressive-controlled column failures considered in this study, for which the AASHTO code was not calibrated. The significantly higher NL reliability index values for the columns are primarily due to the code-specified column reduction factors of 0.75 and 0.80 (to produce an effective combined strength reduction factor of 0.60), as opposed to the less severe tension-controlled strength reduction factor for tension-controlled beams of 0.90. When the column is strengthened with SFRP, no significant difference in axial load reliability results. This is because the column is half-wrapped near the bottom only, and provides no increase in compressive capacity for the upper half of the column.

The effect of including gravity load failures with blast load failures on reliability depends on the blast and axial load levels applied. For the DL and NL load levels, including gravity load failures, within the range of blast loads considered, has no significant effect on the overall failure probability in nearly all cases. For example, considering the case where failure probabilities between these two cases (i.e. values shown in Table 2 and those for a corresponding column in Figures 11 - 16) are closest, which would cause the greatest change in reliability when these two modes are combined, is for a $\rho = 0.015$, 55 MPa column wrapped with SFRP at the NL load level exposed to a scaled blast distance of $Z = 0.23$ m/kg$^{1/3}$, with a reliability index of $\beta = 4.75$, as shown on Figure 9). Per Table 2, the corresponding axial-load only reliability index for this column is β

= 4.58. The resulting reliability index when both failure modes are included is approximately 4.53, or a 5% decrease from the blast load only reliability index shown in Figure 9. The next most-affected result is the 42 MPa column but otherwise the same as the 55 MPa column case above, where reliability index was found to be approximately 3% lower than shown in Figure 9. For all other cases shown on the Figures, differences in reliability due to including the initial gravity load failures were less than 1% from the values shown.

In contrast, for the ML load level, including gravity overload failures with blast failures will have a profound effect on column reliability level. Unlike the DL and NL load levels, which have relatively high reliability under axial load only, reliability under axial load is close to zero due the extreme value of the ML gravity load imposed. Combining this high initial failure probability with blast load results in all ML cases with reliability close to or below zero (values ranged from $-1.47 \leq \beta \leq 0.12$), where reliability decreases as scaled distance Z decreases on all cases. These reliability levels are so low as to be beyond practical interest, and were not investigated further.

For comparison to current code standards, note that that minimum acceptable reliability index for bridge members according to the AASHTO LRFD Specifications is 3.5 (Nowak 1999). For the columns and blast scenarios studied, consider those subjected to the most likely (and conservative) DL axial load condition. To meet the minimum reliability target of 3.5, columns with no SFRP applied can be subjected to Z values from 0.23-0.28 m/kg$^{1/3}$, depending on concrete strength and reinforcing ratio. With SFRP, the scaled distance can be decreased to 0.19-0.26 m/kg$^{1/3}$ while meeting the same level of reliability. Although these differences appear small, they represent substantial changes in charge weight for a given distance. For example, considering a closely placed charge at 1 m from the column face, the equivalent change in weight varies by a factor of 1.2-1.75, where larger increases in charge weight occur for columns with higher concrete strengths and reinforcing ratios.

It should be noted that the reliability analyses assume that the given column material and geometric characteristics are as-specified at the time of blast exposure. That is, depending on environmental exposure, actual column strength may be expected to deteriorate over time. Although the degree of deterioration is generally governed by the inspection, maintenance, and repair strategies of the agency, it is certainly possible that a deteriorated column may experience a blast event prior to a full repair. Such potential decreases in strength are not accounted for in the results presented. However, general reductions in concrete strength and steel area (due to corrosion) might be indirectly accounted for in the results provided by taking inputs on the graphs of concrete strength and reinforcing ratio as effective values at the time considered (e.g. using a reduced steel area due to corrosion) rather than nominal values, interpolating results between the given curves as needed. Another issue to consider is that FRP is typically used to retrofit columns that may have previously experienced damage from deterioration, impact, or another source. In this case, modeling the type of repair may become critical to assess performance under blast load. For example, the extent of the existing concrete surface that was removed, and the quality of bond between the old and new cementitious materials may become important considerations.

Conclusions

The reliability of typical reinforced concrete bridge columns externally strengthened with SFRP and exposed to blast and gravity load was investigated. Columns behavior was represented with a finite element model that accounted for cumulative damage, fracture, and element separation. A variety of concrete strengths, reinforcement ratios, and load levels were studied, while uncertainties in material strength, stiffness, as load parameters were considered in the probabilistic analysis. Specific results of the study are as follows:

- For the columns and blast scenario considered, reliability under blast is most significantly increased by raising concrete strength, followed by SFRP wrapping, then by increasing steel reinforcing ratio.
- Because increasing axial load on a short column enhances resistance to lateral blasts, neglecting axial load provides a conservative assessment of blast reliability.
- The degree to which SFRP wrapping benefits column reliability varies with blast level and column characteristics, where greater enhancements generally occur for lower blast loads and higher strength columns.
- For the cases considered, strengthening columns with SFRP enables maintaining a reference reliability index of 3.5 while subjected to decerases in scaled distance from approximately 5-20%. These differences represent subtaintal increases in allowed charge weight at close distance.
- Because SFRP wrapping is a relatively inexpensive, fast, and unobtrusive retrofit option, results of this study suggest that it may be a viable option for blast protection of existing bridge columns when maintaining a given level of reliability is of concern. Although bridge blast loading is mentioned in AASHTO LRFD and was considered in other studies, currently, such an event does not appear to be a substantial threat in the United States. Given the beneficial results of SFRP wrapping suggested by this study, it may be worthwhile to further explore the effectiveness of this strengthening method to mitigate damage from vehicular impacts as well, which may pose a higher level of risk.

References

AASHTO. (2017). *LRFD Bridge Design Specifications*, 8th Ed., Washington, D.C.

Acar, E., Rais-Rohani, M., and Eamon, C. (2008). "Reliability Estimation Using Univariate Dimension Reduction and Extended Generalized Lambda Distribution." *International Journal of Reliability and Safety*, 4:166-87.

Alsendi, A., and Eamon, C. (2020) "Quantitative Resistance Assessment of SFRP-Strengthened RC Bridge Columns Subjected to Blast Loads." *ASCE J. of Performance of Constructed Facilities*, 10.1061/(ASCE)CF.1943-5509.0001458.

Anwarul Islam, A., and Yazdani, N. (2008). "Performance of AASHTO girder bridges under blast loading." *Engineering Structures*, 30:1922-37.

Atadero, R.A., and Karbhari, V.M. (2008) "Calibration of resistance factors for reliability based design of externally-bonded FRP composites." *Composites Part B Engineering*, 39:665-79.

Au, SK., and Beck, JL. (2001) "Estimation Of Small Failure Probabilities In High Dimensions By Subset Simulation." *Probabilistic Engineering Mechanics*, 16:263-77.

Bai, Y., and Jin, W. (2016). Marine Structural Design, *second edition*.

Behnam, B., and Eamon, C. (2013) "Reliability-Based Design Optimization of Concrete Flexural Members Reinforced with Ductile FRP Bars." *Construction and Building Materials*, 47:942-50.

Cofer, W., Matthews, D., and McLean, D. (2010). "Effects of blast loading on prestressed girder bridges." *Shock and Vibration*, 19(1):1-18.

Eamon, C., Baylot, J., and O’Daniel, J. (2004). “Modeling Concrete Masonry Walls Subjected to Explosive Loads.” *ASCE Journal of Engineering Mechanics*, 10.1061/(ASCE)0733-9399(2004)130:9(1098).

Eamon, C., and Charumas, B. (2011). “Reliability Estimation of Complex Numerical Problems using Modified Conditional Expectation Method.” *Computers and Structures*, 89:181-88.

Eamon, C., Darwish, I., and Alsendi, A. (2018). “Development of Secondary Route Bridge Design Plan Guides.” Michigan Department of Transportation Report SPR-1669.

Eamon, C., Kamjoo, V., and Shinki, K. (2016). “Design Live Load Factor Calibration for Michigan Highway Bridges.” *ASCE Journal of Bridge Engineering*, 21:04016014.

Eamon, C., Kamjoo, V., and Shinki, K. (2014). “Side By Side Probability for Bridge Design and Analysis.” *Michigan Department of Transportation Report RC-1601*.

Eamon, C., Patki, K., and Alsendi, A. (2020). “Failure Sampling with Optimized Ensemble Approach for the Structural Reliability Analysis of Complex Problems.” *ASCE-ASME Journal of Risk and Uncertainty in Engineering Systems, Part A: Civil Engineering*.

Ellingwood, B., Galambos, T.V., MacGregor, J.G., and Cornell, C.A. (1980). “Development of a Probability Based Load Criterion for American National Standard A58.” NBS Special Report 577. Department of Commerce, National Bureau of Standards. U.S; 1980.

Foglar, M., Hajek, R., Fladr, J., Pachman, J., and Stoller, J. (2017). “Full-scale experimental testing of the blast resistance of HPFRC and UHPFRC bridge decks.” *Construction and Building Materials*, 145:588-601.

Foglar, M., and Kovar, M. (2013). “Conclusions from experimental testing of blast resistance of FRC and RC bridge decks.” *International Journal of Impact Engineering*, 59:18-28.

Fujikura, S., and Bruneau, M. (2011). “Experimental investigation of seismically resistant bridge piers under blast loading.” *ASCE Journal of Bridge Engineering*, 10.1061/ (ASCE)BE.1943-5592.0000124.

Gomes, HM., and Awruch, AM. (2004). “Comparison of Response Surface and Neural Network with Other Methods for Structural Reliability Analysis.” *Structural Safety*, 26:49-67.

Hao, H., Li, Z., and Shi, Y. (2016). "Reliability analysis of RC columns and frame with FRP strengthening subjected to explosive loads.” *ASCE Journal of Performance of Constructed Facilities*, 30: 04015017.

Hao, H., Stewart, M., Li, Z., Shi, Y. (2010). "RC column failure probabilities to blast loads.” *International Journal of Protective Structures*, 1:571-91.

Hardwire Armor Systems: Hardwire tapes. Pocomoke City MD. https://www.hardwirellc.com, accessed 2014.

Heffernan, P., Wight, G., and Erki, M.-A. (2011). “Research on the Use of FRP for critical load-bearing infrastructure in conflict zones.” *ASCE Journal of Composites for Construction*, 10.1061/(ASCE)CC.1943-5614.0000077.

Holmquist, T., Johnson, G., and Cook, W. (1993). “A computational constitutive model for concrete subjected to large strains, high strain rates, and high pressures.” *Proc., 14th International symposium, Warhead mechanisms, terminal ballistics; 1993; Quebec; Canada*, 2:591-600.

Hyde, D. (1988). *User's Guide for Microcomputer Program CONWEP, Applications of TM 5-855-1*, Fundamentals of Protective Design for Conventional Weapons. SL-88-1, U.S. Army Corps of Engineers Waterways Experiment Station Instruction, Vicksburg, MS.

Kingery, C., and Bulmash, G. (1984). *Air-Blast Parameters from TNT Spherical Air Burst and Hemispherical Surface Burst*. ARBRL-TR-02555, U.S. Army Ballistic Research Laboratory, Aberdeen Proving Ground, MD.

Lawver, D., Daddazio, R., Oh, G. J., Lee, C.K.B., Pifko, A. B., and Stanley, M. (2003). "Simulating the response of composite reinforced floor slabs subjected to blast loading." *Proc., 2003 ASME International Mechanical Engineering Congress, ASME, New York*, 10.1115/IMECE2003-43870.

Livermore Software Technology Corporation. (2018). *LS-DYNA keyword user's manual, version 971*, Livermore, CA.

Malvar, L., Crawford, J., and Morrill, K. (2007). "Use of composites to resist blast." *ASCE Journal of Composites for Construction*, 10.1061/(ASCE)1090-0268(2007)11:6(601).

Nowak, A.S. (1999) "Calibration of LRFD bridge design code." *NCHRP Report 368, Transportation Research Board*, Washington, D.C.

Nowak, A.S., and Szerszen, M.M. (2003) "Calibration of Design Code for Buildings (ACI 318): Part 1-Statistical Models for Resistance." *ACI Structural Journal*, 100:377-82.

Nowak, A.S. and Eamon, C. (2008). "Reliability Analysis of Plank Decks." ASCE Journal of Bridge Engineering, 13(5): 540-546.

Patki, K., and Eamon, C. (2016). “Evaluation of Alternative Implementation Methods of Failure Sampling Approach for Structural Reliability Analysis.” *ASCE-ASME Journal of Risk and Uncertainty in Engineering Systems, Part A: Civil Engineering*, 2:04016004.

Rackwitz, R., and Fiessler, B. (1978). “Structural Reliability Under Combined Random Load Sequences.” *Computers and Structures*, 9:484-94.

Rocha, D., Eamon, C., and Murphy, J. (2011) “Reliability Analysis of Roof Sheathing Panels Exposed to a Hurricane Wind.” *Structural Safety*, 33:74-81.

Shi, Y., and Stewart, M. (2015). "Spatial reliability analysis of explosive blast load damage to reinforced concrete columns.” *Structural Safety*, 53:13-25.

Sikadur-30 (2017). "Thixotropic epoxy adhesive for bonding reinforcement.” *Product data sheet*, version 02.01, Welwyn Garden City, Hertfordshire, UK.

Thomas, R., and Sorensen, A. (2018). "Reliability analysis of circular reinforced concrete columns subjected to sequential vehicular impact and blast loading.” *Engineering Structures*, 168:838-51.

Val, D., and Chernin, L. (2009). “Serviceability Reliability of Reinforced Concrete Beams with Corroded Reinforcement.” *Journal of Structural Engineering*, 135:896-905.

Williamson, E., Bayrak, O., Davis, C., and Williams, G. (2011a). “Performance of bridge columns subjected to blast loads. I: experimental program.” *ASCE Journal of Bridge Engineering*, 10.1061/(ASCE)BE.1943-5592.0000220.

Williamson, E., Bayrak, O., Davis, C., and Williams, G. (2011b). “Performance of bridge columns subjected to blast loads. II: results and recommendations.” *ASCE Journal of Bridge Engineering*, 10.1061/(ASCE)BE.1943-5592.0000221.

Williams, G., and Williamson, E. (2011). “Response of reinforced concrete bridge columns subjected to blast loads.” *ASCE Journal of Bridge Engineering*, 10.1061/ (ASCE)ST.1943-541X.0000440.

Wisniewski, D., Cruz, P., Henriques, A., and Simoes, R. (2012). “Probabilistic Models for Mechanical Properties of Concrete, Reinforcing Steel and Pre-stressing Steel.” *Structure and Infrastructure Engineering*, 8:111-23.

Winget, D., Marchand, K., and Williamson, E. (2005). “Analysis and design of critical bridges subjected to blast loads.” *ASCE Journal of Bridge Engineering*, 10.1061/(ASCE)0733-9445(2005)131:8(1243).

Yi, Z., Agrawal, A., Ettouney, M., and Alampalli, S. (2014a) “Blast load effects on highway bridges. I: modeling and blast load effects.” *ASCE Journal of Bridge Engineering*, 10.1061/(ASCE)BE.1943-5592.0000547.

Yi, Z., Agrawal, A., Ettouney, M., and Alampalli, S. (2014b) “Blast load effects on highway bridges. II: failure modes and multihazard correlations.” *ASCE Journal of Bridge Engineering*, 10.1061/(ASCE)BE.1943-5592.0000548.

List of Tables

List of Figures

Table 1. Random Variables.

Random Variable (RV)	Total	Nominal value	Bias factor*	V**
Resistance RVs				
Concrete strength (f'_c)	1	28-55 MPa	1.15	0.15
Yield stress, long. bars (F_{yl})	24	414 MPa	1.14	0.05
Yield stress, ties (F_{yt})	1	276 MPa	1.145	0.05
Yield stress, SFRP steel fibers (F_{yS})	1	985 MPa	1.14	0.03
Young's Modulus, long. bars (E_l)	24	200 GPa	1.0	0.04
Young's Modulus, ties (E_t)	1	200 GPa	1.0	0.04
Young's Modulus, SFRP(E_S)	1	66.1 GPa	1.0	0.04
Tangent modulus, long. bars (E_{Tl})	24	20 GPa	1.0	0.04
Tangent modulus, ties (E_{Tt})	1	20 GPa	1.0	0.04
Tangent modulus, SFRP (E_{Ts})	1	98.5 MPa	1.0	0.04
Load RVs (load on column)				
Weight, prefab items (D_p)	1	67 kN	1.03	0.08
Weight, cast in place items (D_s)	1	387 kN	1.05	0.10
Weight, wearing surface (D_w)	1	134 kN	mean=89 mm	0.25
Gravity load, vehicular traffic (LL)	1	145 kN	1.3-2.3	0.11-0.18
Charge weight (Q_w)	1	50-600 kg	1.0	0.10
Equivalency factor (Q_e)	1	1.00	mode=0.82	0.36

*Ratio of mean to nominal value. Vehicle load bias factor given in terms of two-lane HS-20 live load.
**Coefficient of variation.

Table 2. Column Reliability Index Under Axial Load Only.

Column	DL	NL	ML
ρ = 0.015, f'_c = 28	8.15	5.05	0.116
ρ = 0.015, f'_c = 42	7.66	4.74	0.114
ρ = 0.015, f'_c = 55	7.42	4.58	0.113
ρ = 0.029, f'_c = 28	9.77	5.96	0.121
ρ = 0.029, f'_c = 42	8.77	5.37	0.118
ρ = 0.029, f'_c = 55	8.26	5.06	0.116
ρ = 0.042, f'_c = 28	10.2	6.70	0.124
ρ = 0.042, f'_c = 42	9.76	5.92	0.121
ρ = 0.042, f'_c = 55	9.01	5.49	0.119

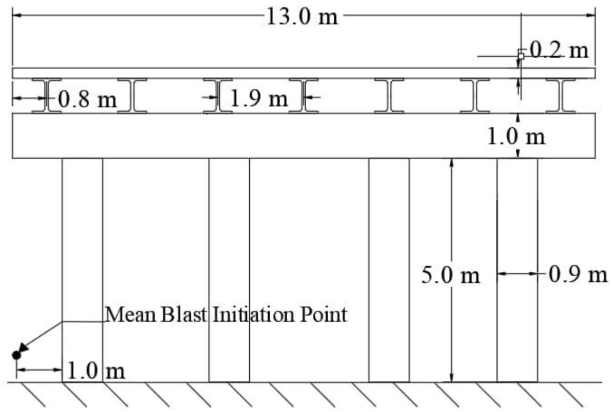

Figure 1. Bridge Pier Considered.

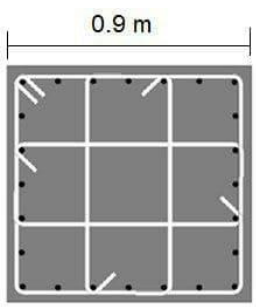

Figure 2. Column Cross-Section Considered.

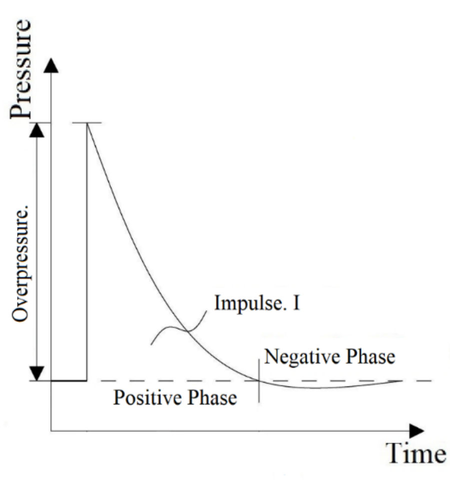

Figure 3. Typical Blast Pressure Curve.

Figure 4. Comparison of Experimental and FEA Results (Alsendi and Eamon 2020; Williamson et al. 2011).

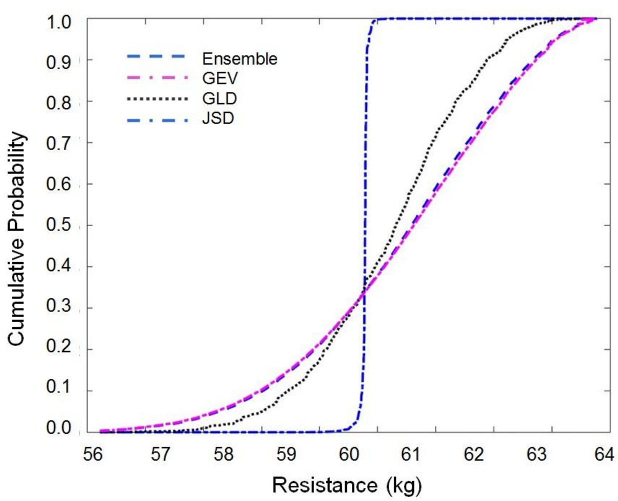

Figure 5. Example CDF Ensemble of Column Resistance.

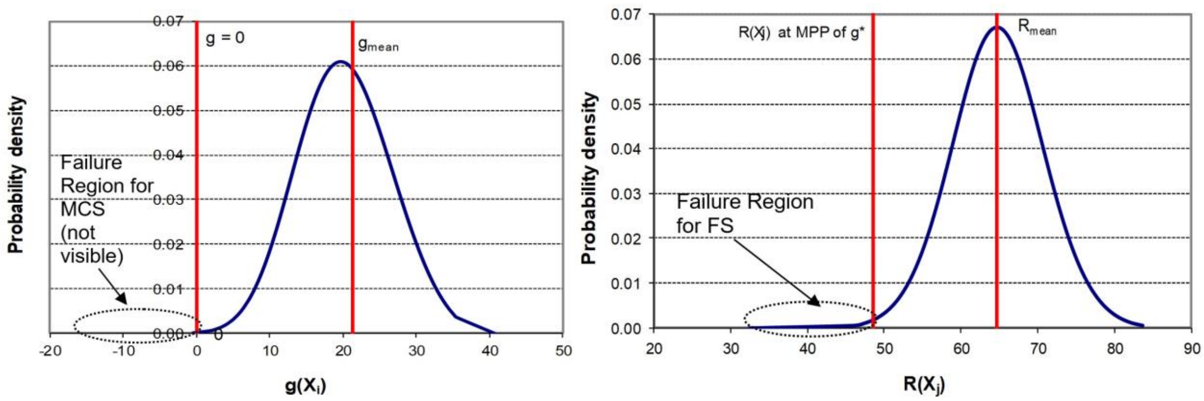

Figure 6. Illustration of Direct MCS vs FS Approach (Problem with β= 3.31).

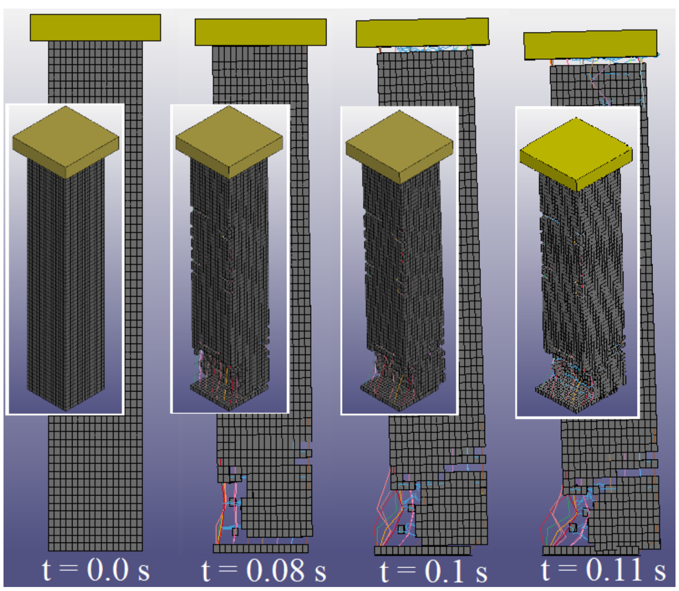

Figure 7. Typical Response of Column to Blast.

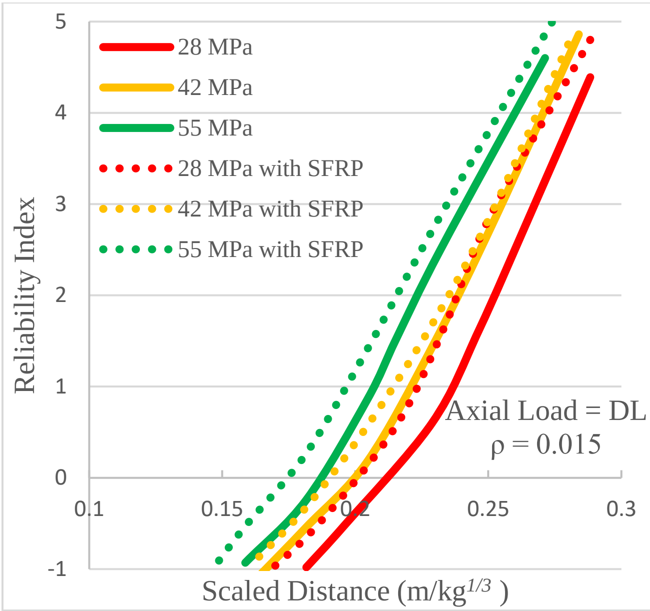

Figure 8. Column Reliability, ρ = 0.015, DL Load Case.

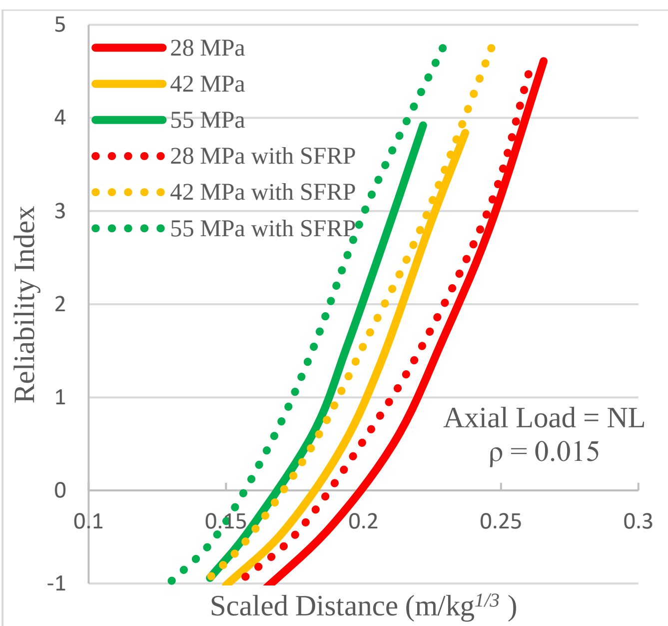

Figure 9. Column Reliability, ρ = 0.015, NL Load Case.

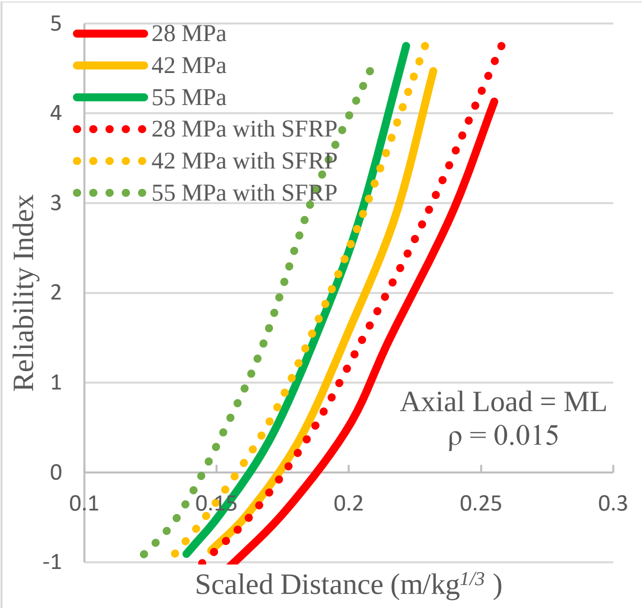

Figure 10. Column Reliability, ρ = 0.015, ML Load Case.

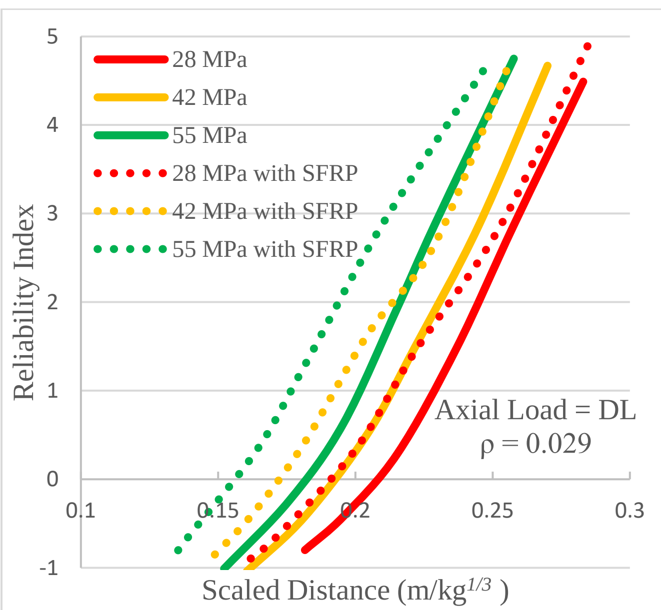

Figure 11. Column Reliability, ρ = 0.029, DL Load Case.

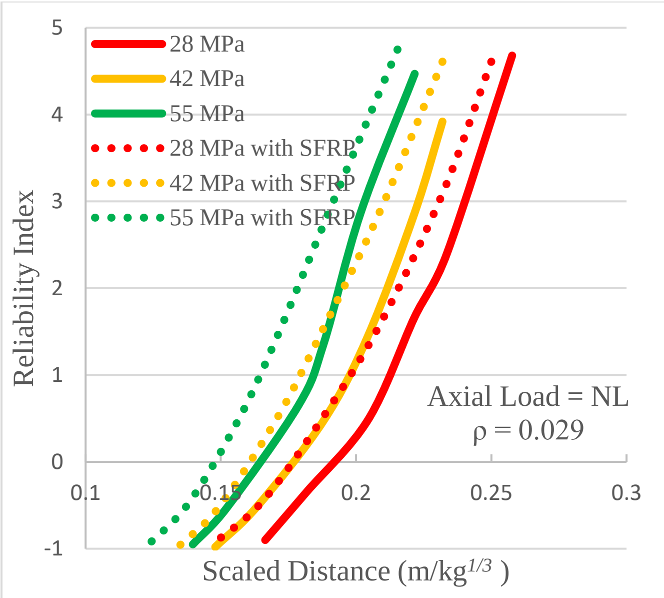

Figure 12. Column Reliability, ρ = 0.029, NL Load Case.

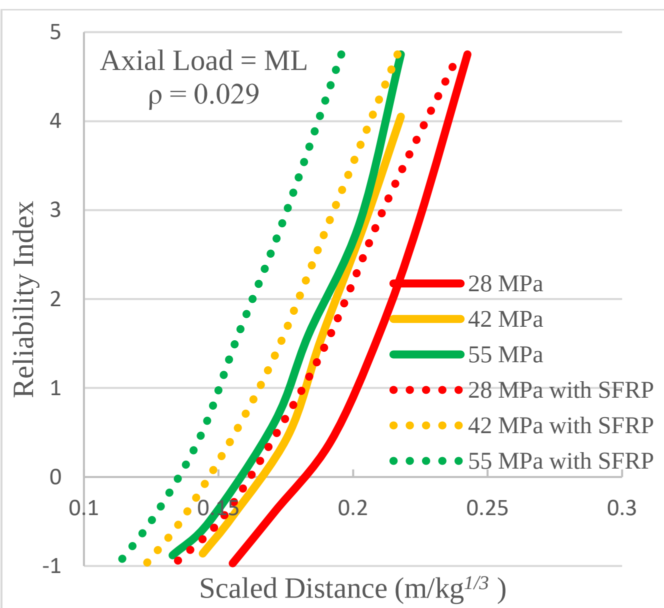

Figure 13. Column Reliability, ρ = 0.029, ML Load Case.

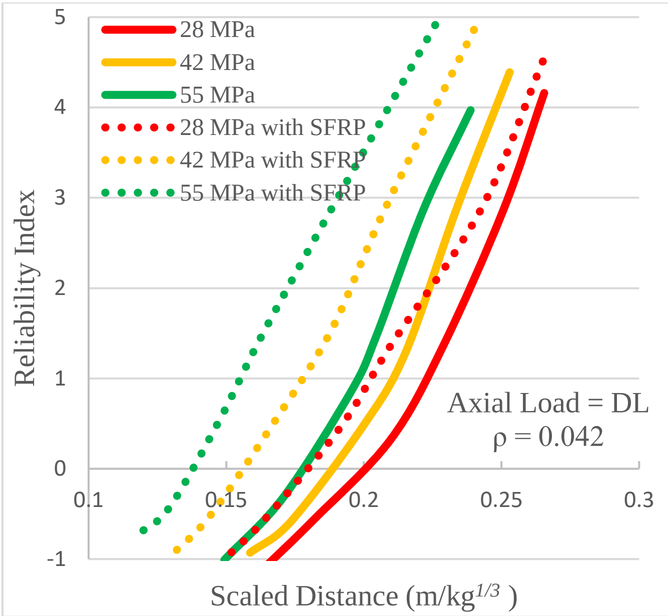

Figure 14. Column Reliability, ρ = 0.042, DL Load Case.

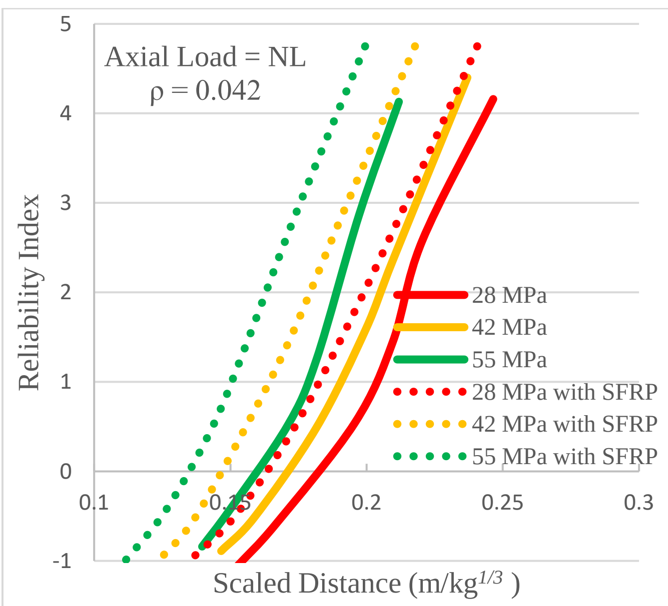

Figure 15. Column Reliability, ρ = 0.042, NL Load Case.

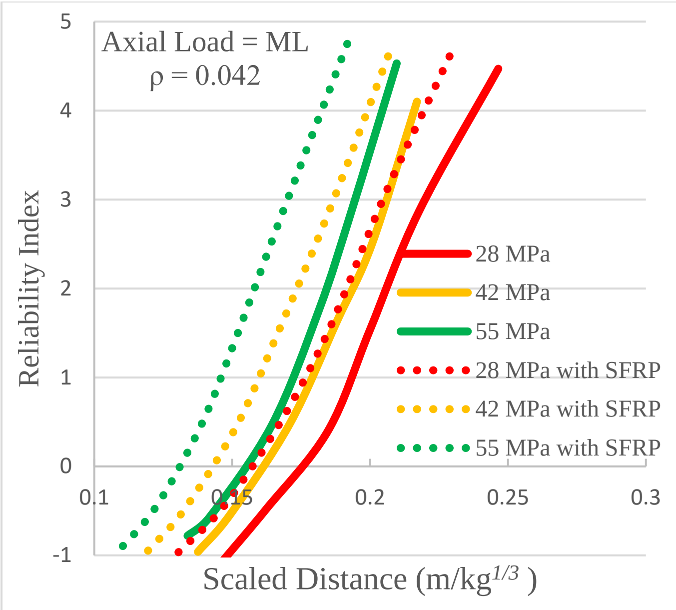

Figure 16. Column Reliability, ρ = 0.042, ML Load Case.